Proceedings of the ASME 2016 International Mechanical Engineering Congress & Exposition
IMECE 2016
November 13-19, 2016, Phoenix, Arizona, United States

IMECE2016-65405

DYNAMIC FOCUSING OF ELECTROSPINNING PROCESS WITH QUADRUPOLE TRAPS

Rudolf Kyselica and Eniko T. Enikov*
Advanced Micro- and Nanosystems Laboratory
Department of Aerospace and Mechanical Engineering
University of Arizona
Tucson, Arizona 85721
Email: enikov@email.arizona.edu

ABSTRACT

Electrospinning is the most widely used production method for polymer fibers formed from an electrified fluid jet. This method is very versatile, relatively inexpensive and simple. When the sufficiently high electric potential (about 20kV) is applied to the polymer solution, the electrostatic forces overcome the surface tension of the polymer and a thin liquid jet is ejected from the nozzle. However, after short straight distance of the motion of the fiber it rapidly grows into an electric charge driven bending instability and results in a 3D spiraling trajectory leading to a very random deposition on the grounded collector. This significantly reduces the positive qualities of the fiber and its use in biomechanical engineering like a production of tissue scaffolds mimicking the structure of the extracellular matrix or a delivery of expandable chemo- and radio-therapeutic stents. In this work we present the initial results from investigating the feasibility of using dynamic focusing of the electrified jet in a linear quadrupole trap. This is a new alternative to the more generally used mechanical approach with rotating mandrel, could in principle lead to the ability to control the deposition location without the use of any moving components. The proposed approach was originally developed for trapping and transporting individual charged ions. In contrast to ions, an electrified continuous fiber represents an infinite degree of freedom system, with potentially much richer dynamics and unknown stability regions in the parameter space.

In order to understand the dynamics of the fiber, we present a discretized 2D reduced- order mathematical model which is investigated numerically. The resulting ODEs represent multi-dimensional form of a non-linear Mathieu's and Meissner's differential equations for harmonic, and step excitation functions, respectively. The model parameters were obtained from static experiments with electrodes compressing the fibers in a single plane. Finite-element model of the electrodes resulted in detailed potential maps, which were used to develop estimates of the required strength of the electrostatic field needed to steer the fibers.

The estimated parameters were used to obtain stable solutions of the reduced-order approximate of a spring-mass-charged dumbbell model of the fiber.

INTRODUCTION

Electrospinning has emerged as a simple method for production of nanofibers [1, 2]. However, because the produced fiber strongly depends on many parameters, it is quite difficult to have its production completely under control and produce the fiber of specific material properties. Generally, straightness and orientation of the fiber are most difficult to control because of the bending and buckling instabilities of the fiber. This is the reason why the majority of the produced nanofibers are unstructured and disordered. Such random deposition patterns prevent the use of the resulting fiber mats into expandable tissue scaffolds or stents [3]. The most common method for fiber alignment is to use a fast

*Address all correspondence to this author.

moving collector (mandrel/drum) which is spinning and winding the fiber around its perimeter. If the collector velocity is sufficiently large, the fiber is straightened as it is being collected. This principle was very well adopted by many researchers and companies producing the nanofibers, however it requires additional work to stack and shape the fiber to obtain the needed pattern or design [4]. Also the deposited fiber lands on large surfaces resulting in small surface density.

An alternative approach would be to use the fiber properties, namely its electric charge, and control its movement and deposition by electric field [5]. From Earnshaws theorem (1842) it is known, that a static collection of point charges cannot be maintained in a stable stationary equilibrium configuration solely by the electrostatic interaction of the charges. This means the fiber could not be controlled by static electric field. Instead, multi-pole traps utilzie time-varying electric field that under the correct frequency and amplitude results in confinement of the charges to a small volume. In the absence of dynamic rotation of the electrostatic field, the charges are compressed in one direction and repelled in the transversal direction due as demonstrated in a previous two-electrode experiment shown in Fig. 1.

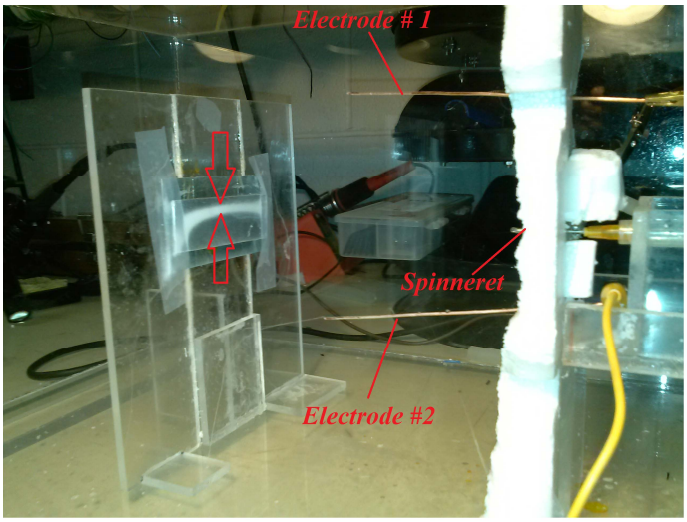

FIGURE 1. Wire electrode focusing design with nozzle on the right, collector plate on the left and 2 electrodes symmetrically placed in vertical plane.

While the fiber appears aggregated in the horizontal plane, under a microscope examination is it visible that the individual fibers are still curly and meandering. To dynamically stabilize the fiber a second pair of electrodes are required so that the fiber can be confined in both horizontal and vertical planes. The collection of four cylindrical electrodes along the extrusion axis form a linear quadrupole trap with harmonically changing electric field.

LINEAR QUADRUPOLE TRAP

The working principle of a linear quadrupole trap [6] is conceptually simple. The fiber at the point of its creation is highly charged by electric voltage applied on the nozzle (20-30 kV). The quadrupole trap is placed in its trajectory in such a way, that the fiber needs to pass through it before it can get to the collector. These electrodes are symmetrically placed along the trap axis with 180 degrees between electrodes of the same potential as depicted on a Fig. 2 One electrode pair of the trap is charged

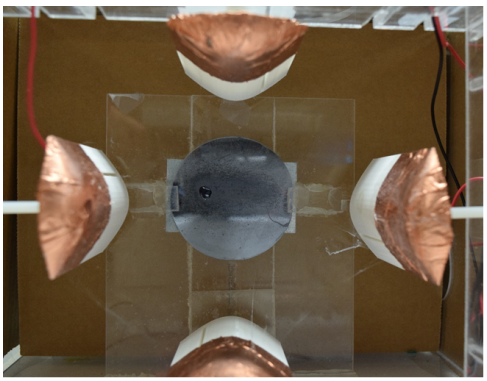

FIGURE 2. Quadrupole linear trap design - view in the direction of travel of the fiber from nozzle to the collector plate.

with constant voltage of certain value (here called offset voltage) and the other electrode pair is powered by an AC voltage of sine or square waveform with min a given amplitude above and below the offset voltage. Thus its potential varies by the value of the amplitude above and below the first pari of electrodes.

Figure 3 shows the an example of the resulting electric field lines and fiber propagation direction for an offset voltage of 8 kV and amplitude of 2 kV.

As the fiber gets into the electric field of the linear quadrupole trap, the trap influences its direction of movement in such a way, that it attracts the fiber to the electrode pair with lower electric potential during half of the oscillation period (top half of Fig. 3). If the period is selected properly, before the fiber reaches the electrode‘s surface, the voltage on AC electrode pair changes and so that the attractive forces draw the fiber th the other pair (bottom half of Fig. 3). The electric field keeps changing with the frequency of the AC voltage applied to the electrodes and forcing the fiber to travel in a spiral until it is collected on a collector. By controlling the frequency and voltage setting, it is anticipated that a stable regime can be established. The following sections are devoted to development of numerical

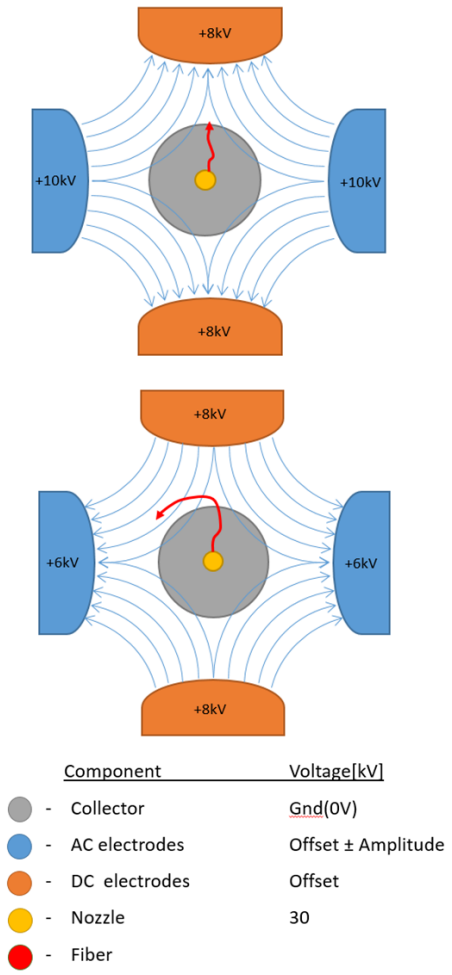

FIGURE 3. Working principle of the quadrupole trap

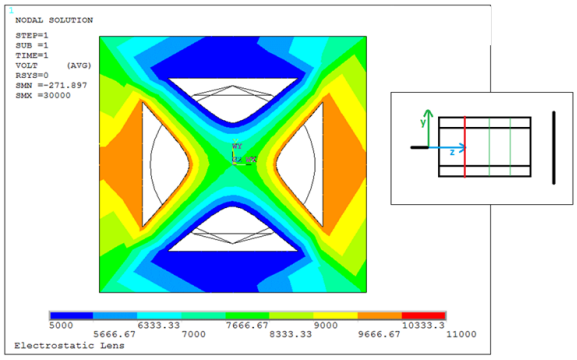

FIGURE 4. Voltage [V] map inside of the quadrupole trap - 1st quarter of the legth of the trap

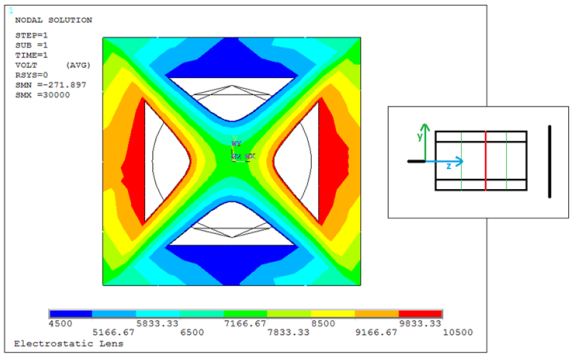

FIGURE 5. Voltage [V] map inside of the quadrupole trap - middle of the legth of the trap

evidence of such stable operation using a reduced-order model of the fiber dynamics.

ELECTRIC FIELD CALCULATION

To be able to model the behavior of the fiber inside the electric field created by the linear quadrupole trap, properties of this electric field had to be calculated. To obtain the electric field and voltage map inside of the trap, static analysis in ANSYS, APDL was created. Figures 4-6 represent voltage distributions in [kV] in 3 cross-sections of the quadrupole trap. Planes in which voltages are plotted cut the quadrupole into quarters, starting from the side closer to the nozzle. This is plotted for offset voltage =10KV and amplitude=5kV.

Figure 7 shows the variation of the electric field E_y [V/m] in y (vertical) direction. A nearly linear variation is observed int the central portion of the trap near the z-axis. ($x = 0, y = 0$). Only a half of the trap is plotted as the electric field in y direction inside of the trap is symmetric with respect to the x-z plane but of opposite orientation. The vertical plane in which electric field is plotted is in the middle of the length of the trap.

Also from the Fig. 8 we can see the electric field in y direction (purple line) along the axis of the trap for position offset from the axis of the trap by 10 mm in y direction as shown on Fig. 9

From the obtained electric field, one can estimate the centering force acting on the fiber through

$$F_x = E_{xx}\, q\, x \cos(\omega t)\,, \tag{1}$$

where E_{xx} is the static amplitude of the electric field gradient in the x direction, q is the electrostatic charge of a segment of the fiber with length l. The electrostatic charge can be estimated from the electrospinning current, I and the velocity of the fiber v

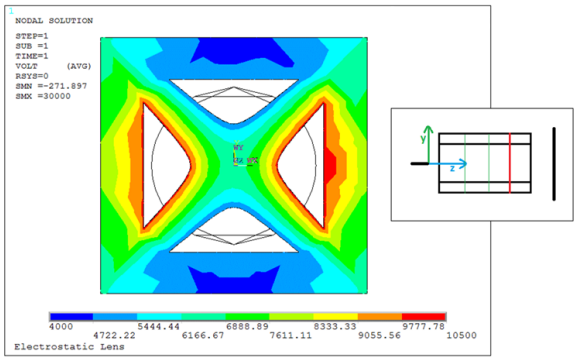

FIGURE 6. Voltage [V] map inside of the quadrupole trap - 3rd quarter of the legth of the trap.

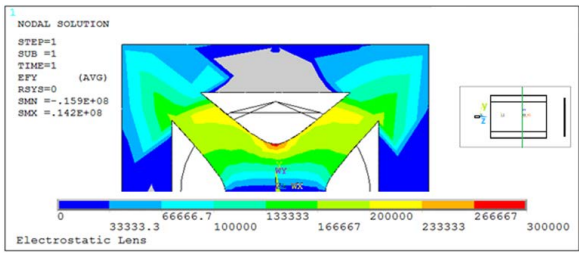

FIGURE 7. Electric field [V/m] in y direction inside of the upper half of the quadrupole trap - in the middle of the legth of the trap.

through

$$q = \frac{Il}{v}. \tag{2}$$

To verify the value of the electric field gradient, point measurements of the electrostatic potential were carried out on a grid of test points within the upper half of the vertical plane along the axis of the trap. Figure 10 shows the resulting equipotential lines. Fig. 11 shows the simulation results for the same wire electrode model and we can see the equipotential lines (edges of each of the color fields) are very similar what proves the correctness of the simulation.

MATHEMATICAL MODELS AND SIMULATIONS

The analysis of the dynamics of the fiber were examined through series of several models of increasing complexity. The first model is a simplified one-dimensional 1-DOF model of a fiber to examine the effect of a a half of the quadrupole trap and develop an order-of-magnitude estimate of the resulting forces. This model can be seen on Fig. 12. The corresponding equation

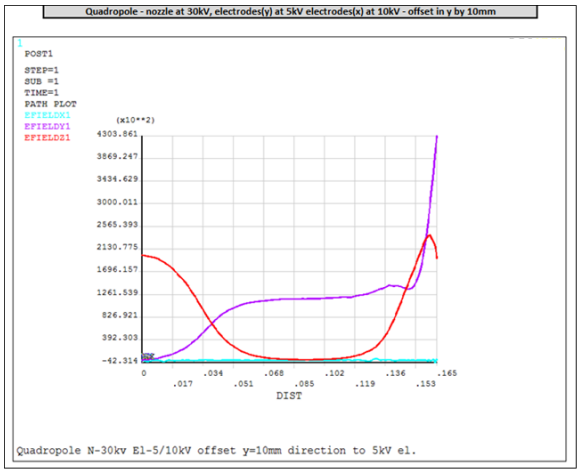

FIGURE 8. Electric field [V/m] inside of the quadrupole trap - offset 10mm in y direction.

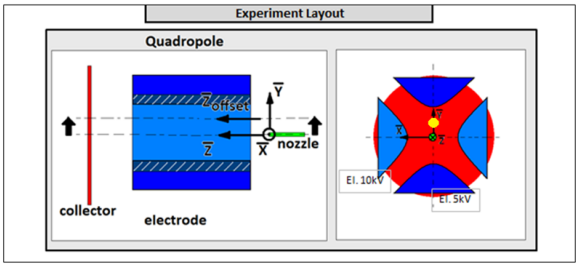

FIGURE 9. Model of the trap used for electric field simulation with marked offset from the center line of the trap.

of motion of the system is described by Eqn. (3), which is rewritten in a more-familiar form of Eqn. (4).

$$\ddot{x}m + c\dot{x} + 2kx\left(1 - \frac{l}{\sqrt{l^2+x^2}}\right) = A\cos(\omega t) \tag{3}$$

$$\ddot{x} + x\left(\frac{2k}{m} - \frac{2kl}{m\sqrt{l^2+x^2}} + \frac{A\cos(\omega t)}{m}\right) = 0 \tag{4}$$

The latter is a form of a Hill equation with one harmonic mode, which is known as the Mathieu equation. A distinguishing feature of Eqn. (3) is that it has a non-linear stiffness dependence on x.

A common method for examining Mathieu's equation is to re-write it in a non-dimensional-time form, resulting in two pa-

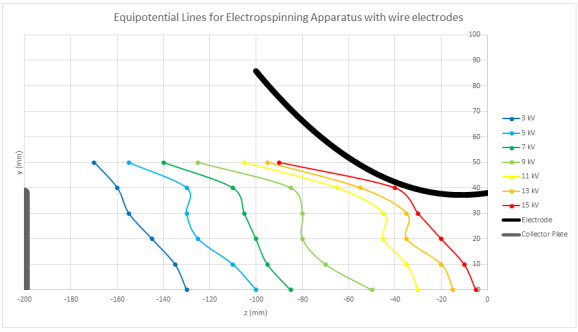

FIGURE 10. Equipotential lines inside of the focusing device with two wire electrodes. Plotted only for upper half as the field is symmetric with respect to a central horizontal plane.

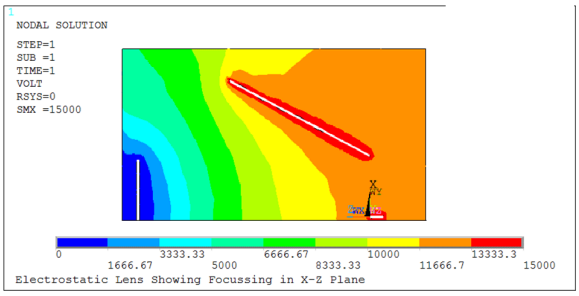

FIGURE 11. Electric Potential [V] calculated inside of the focusing device with two wire electrodes. Plotted only for upper half as the field is symmetric with respect to a central horizontal plane.

rameters q and a [7, 8]. Following this approach, Eqn(4) is re-written into (6) via the transformation

$$\tilde{t} = t\omega \rightarrow d\tilde{t} = dt\,\omega \rightarrow dt = \frac{d\tilde{t}}{\omega}$$
$$\dot{x} = \frac{dx}{dt} = \omega\frac{dx}{d\tilde{t}} \rightarrow x = \omega^2\frac{dx}{d\tilde{t}} = \omega^2\ddot{\tilde{x}} \qquad (5)$$

$$\ddot{\tilde{x}} + \tilde{x}\left[2\frac{k}{m\omega^2} - \frac{2kL}{m\omega^2\sqrt{x^2+L^2}} + \frac{A}{m\omega^2}\cos(\tilde{t})\right] = 0 \qquad (6)$$

It can be seen that for small deflections x, Eqn. (6), results in the classical linear Mathieu equation with parameters a and q

$$\ddot{\mathrm{x}} + x\,(a + q\cos(\omega t)) = 0 \qquad (7)$$

Therefore, it is anticipated that for small amplitudes of oscillations around the axis of the linear trap, the stability of the solu-

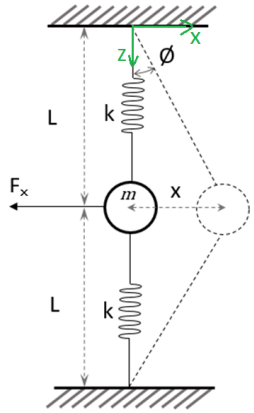

FIGURE 12. 1dimensional, 1DOF simplified model of the fiber

tion will be governed by the stability chart obtained for the linear Mathieu equation. Mathieu equation stability chart (Fig. 13) describes the stable(white) and unstable(hatched) regions. Since the exact material properties of the fiber are not known, its is desirable to choose a parameter pair well within the stability domain of the diagram [9, 10]. The least known parameter is the stiffness of the fiber. It could change due to diameter variations, different amount of solvent during the drying of the fiber as it travels in the air.

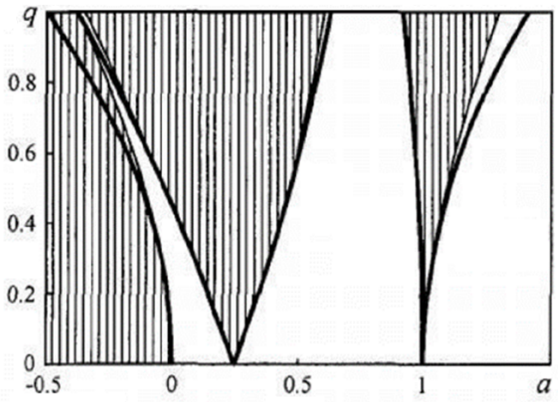

FIGURE 13. Instability domains for the Mathieu's equation, where hatched regions are unstable.

A deficiency of the current model is that it constraints the fiber at its beginning and end points. This constraint is making the system very stiff and quite unrealistic. To relax the constraint, a new model with additional point masses is needed. This model is shown on Fig. 14. The resulting 10-th order differential equa-

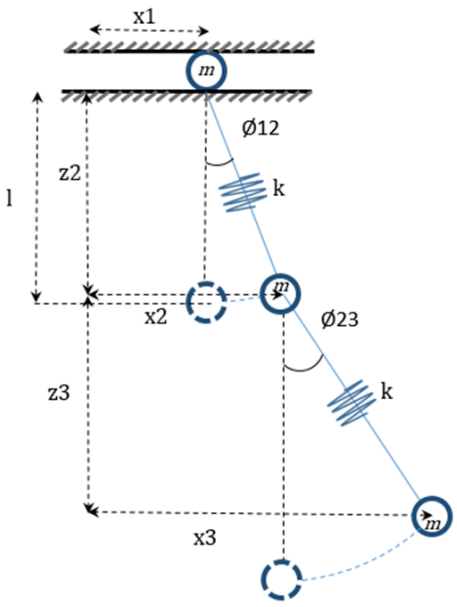

FIGURE 14. Mathematical model of the fiber discretized into 3beads that are free to move in x-z plane-except of the first one that is still constrained in z.

tion is in the form of

$$\dot{\mathbf{x}} = f(\mathbf{x},t), \tag{8}$$

where $f(\mathbf{x},t)$ is periodic in t and contains non-linear stiffness terms such as

$$\frac{kl}{m\sqrt{(\mathrm{x}_1-\mathrm{x}_3)^2+\mathrm{x}_5{}^2}} - \frac{A\cos(\omega t)}{m} - \frac{2k}{m} + \frac{kl}{m\sqrt{(\mathrm{x}_3-\mathrm{x}_7)^2+(\mathrm{x}_5-\mathrm{x}_9)^2}}$$

Material Properties

To be able to run a simulation of Eq.(8), an order-of-magnitude estimation of realistic values of its parameters is needed. The length segment was arbitrarily set to $l = 1e^{-3}m$. The thickness of the fiber that was obtained from the scanning electron microscope (SEM) image of the fiber (Fig.**??**). The average measured value is $d = 3^{-7}m$. The mass of each element was estimated from

$$m = \frac{\pi d^2 l \rho}{4} \tag{9}$$

The density of the fiber at the point where it is being controlled by the electric field was set to be $\rho = 690kg/m^3$. The liquid solution consists only 5% of PEO and the rest is water. As the fiber travels, water is evaporating and only a dry PEO is collected. Density of PEO is about $\rho_{PEO} = 350kg/m^3$ and so the change of density over the traveled distance is quite signifficant. This has strong influence also on the stiffness of the fiber calculated from

$$k = \frac{\pi E d^2}{4l}, \tag{10}$$

where E is a Young's modulus of the PEO [11]. Damping coefficient was estimated from the Stokes drag force for elliptic body. Fiber is not truly an ellipsoid but if the major axis is much bigger than minor axis, the ellipse becomes very thin and long and actually represents fiber quite well. The coefficient of damping is then calculated from

$$c = \frac{32\pi\tilde{a}e^3\nu}{2e+\log\left(-\frac{e+1}{e-1}\right)(3e^2-1)}, \tag{11}$$

where e is an eccentricity calculated as on Eqn. 12, $\tilde{a}$ is a major axis and b is the minor axis of the ellipse. ν is the dynamic viscosity of air and its value is $\nu = 1.983*10^{-5}Pas$.

$$e = \sqrt{1-\frac{b^2}{\tilde{a}^2}} \tag{12}$$

Numerical Results

The calculation was carried out in Matlab using a built-in solver ODE45. Simulation of movement of the fiber based on model from Fig. 14 gave stable behaviour for certain properties of the electric field at given initial conditions, that were chosen to closely represent the probable positions of points on the fiber represented by 3 point masses as they enter the electric field of the linear quadrupole trap.
With the frequency chosen far from natural frequency of the fiber ($f_n = (\frac{k}{m})^{1/2} = 26.5kHz$) f=60Hz and initial conditions given by (13-14)

$$x(0) = [1e-7,\ 0,\ -1e-7,\ 0,\ l,\ 0,\ 1e-7,\ 0,\ 2*l,\ 0]' \tag{13}$$

where

$$x = [x_1,\ \dot{x}_1,\ x_2,\ \dot{x}_2,\ z_2,\ \dot{z}_2,\ x_3,\ \dot{x}_3,\ z_3,\ \dot{z}_3]' \tag{14}$$

The resulting time responses are shown in figures Fig. 15 - 17.

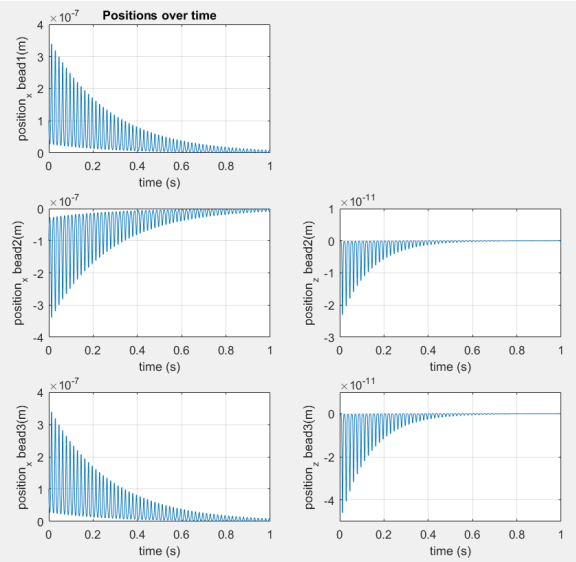

FIGURE 15. Positions of all beads over time in x direction on left and in z direction on right, where z position is reduced by l and so the oscillation about length l is plotted.

As anticipated a frequency of 60Hz was observed in the motion of the beads under the action of the electric field. The position about all beads oscillate over the time converges to 0 indicating that the motion stabilizes on the z axis. This all happens quite fast what is a result of the strong electric field. We can also see that beads are oscillating in z direction as well, however the initial condition in this direction was 0 for all beads. This is caused by the fact that x and y direction movements are bounded and so thy can not move independently from each other.

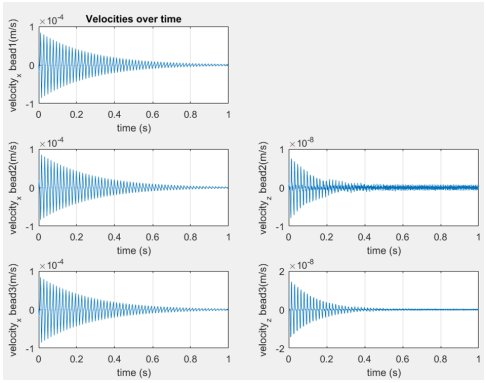

FIGURE 16. Velocities of all beads over time in x direction on left and in z direction on right.

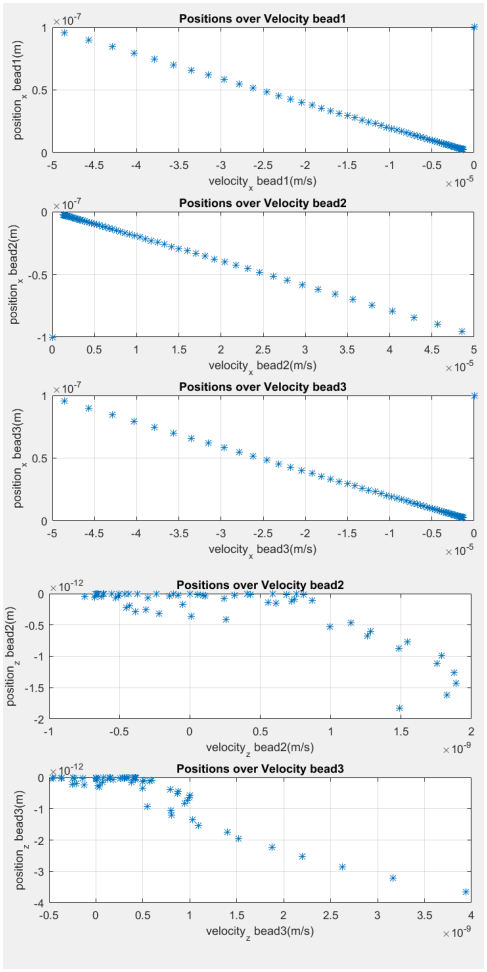

FIGURE 17. Poincare map(plot of x vs $\dot{x}$) for all beads in both x and z direction, where z direction position is reduced by l

Poincaré map ploted on Fig. 17 is showing the position of the bead over its velocity every period T with which it oscillates.

DISCUSSION AND CONCLUSIONS

Several models of the dynamics of electrified fibers in an harmonically oscillating field were presented. The models demonstrated that for small deviations from the central axis, the fibers dynamics follows that of a classical multi-dimensional Mathieu equation with stable solutions near the origin. Model parameters extracted from static experiments resulted in stable operation of the trap for a frequency of 60 Hz using a low-order model of the fiber (10-DOF). Experimental validation of the operation of the trap is currently underway, as well as development of stability chart for the system parameters.

ACKNOWLEDGMENT

The authors acknowledge the support for this research by a Grant# 1462752 from the National Science Foundation.

REFERENCES

[1] Reneker, D. H., and Yarin, A. L., 2008. "Electrospinning jets and polymer nanofibers". *Polymer,* ***49***(10), pp. 2387 – 2425.

[2] Bhardwaj, N., and Kundu, S. C., 2010. "Electrospinning: A fascinating fiber fabrication technique". *Biotechnology Advances,* ***28***(3), pp. 325 – 347.

[3] Ramakrishna, S., Fujihara, K., Teo, W.-E., Yong, T., Ma, Z., and Ramaseshan, R., 2006. "Electrospun nanofibers: solving global issues". *Materials Today,* ***9***(3), pp. 40 – 50.

[4] Grasl, C., Arras, M. M. L., Stoiber, M., Bergmeister, H., and Schima, H., 2013. "Electrodynamic control of the nanofiber alignment during electrospinning". *Applied Physics Letters,* ***102***(5).

[5] Bellan, L. M., and Craighead, H. G., 2006. "Control of an electrospinning jet using electric focusing and jet-steering fields". Vol. 24, AVS, pp. 3179–3183.

[6] Douglas, D. J., Frank, A. J., and Mao, D., 2005. "Linear ion traps in mass spectrometry". *Mass Spectrometry Reviews,* ***24***(1), p. 29.

[7] Ng, L., and Rand, R., 2002. "Bifurcations in a mathieu equation with cubic nonlinearities". *Chaos, Solitons & Fractals,* ***14***(2), pp. 173 – 181.

[8] Ruby, L. "Applications of the mathieu equation". *American Journal of Physics,* ***64***(1).

[9] SHRIVASTAVA, S. K., and PRADEEP, S., 1985. "Stability of multidimensional linear time-varying systems". *Courses and lectures-International centre for mechanical sciences,* ***8***, p. 583.

[10] Seyranian, A. P., and Mailybaev, A. A., 2003. "Multi-parameter stability theory with mechanical applications.". *World Scientific*, p. 420.

[11] Bellan, L. M., Kameoka, J., and Craighead, H. G., 2005. "Measurement of the young's moduli of individual polyethylene oxide and glass nanofibres". *Nanotechnology,* ***16***(8), p. 1095.

[12] Jang, S. S., , William A. Goddard, I., and Kalani, M. Y. S., 2007. "Mechanical and transport properties of the poly(ethylene oxide)poly(acrylic acid) double network hydrogel from molecular dynamic simulations". *The Journal of Physical Chemistry B,* ***111***(7), pp. 1729–1737.

[13] S. Ramesh, Tan Winie, A. A., 2007. "Investigation of mechanical properties of polyvinyl chloridepolyethylene oxide (pvcpeo) based polymer electrolytes for lithium polymer cells". *European Polymer Journal,* ***43***(5), pp. 1963 – 1968.